

Acceleration of Antarctic Circumpolar Current at the Drake Passage during the GRACE era

Chengcheng Yang¹, Xuhua Cheng¹, Duotian Huang¹, Jianhuang Qin¹, Guidi Zhou², and Jiajia Chen¹

¹Hohai University

²College of Oceanography, Hohai University

January 20, 2023

Abstract

Previous studies have identified intense climatic change in the Southern Ocean. However, the response of ACC transport to climate change is not fully understood. In this study, by using in-situ ocean bottom pressure (OBP) records and five GRACE products, long-term variations of ACC transport are studied. Our results confirm the reliability of GRACE CSR mascon product in ACC transport estimation at the Drake Passage. Superimposed on interannual variability, ACC transport exhibits an obvious increasing trend ($1.32 \pm 0.07 \text{ Sv year}^{-1}$) during the GRACE era. Based on results of a mass-conservation ocean model simulation, we suggest that the acceleration of ACC is associated with intensified westerly winds and loss of land ice in Antarctica.

Hosted file

grl_manuscript_1013.docx available at <https://authorea.com/users/573584/articles/620316-acceleration-of-antarctic-circumpolar-current-at-the-drake-passage-during-the-grace-era>

Hosted file

supporting_information_grl_1013.docx available at <https://authorea.com/users/573584/articles/620316-acceleration-of-antarctic-circumpolar-current-at-the-drake-passage-during-the-grace-era>

1
2 **Acceleration of Antarctic Circumpolar Current at the Drake Passage during the**
3 **GRACE era**

4 **Chengcheng Yang¹, Xuhua Cheng^{1,2*}, Duotian Huang¹, Jianhuang Qin^{1,2},**
5 **Guidi Zhou¹, Jiajia Chen¹**

6 ¹Key Laboratory of Marine Hazards Forecasting, Ministry of Natural Resources, Hohai
7 University, Nanjing, China,

8 ²Southern Marine Science and Engineering Guangdong Laboratory(Zhuhai), Zhuhai, China.

9 *Corresponding author: Xuhua Cheng (xuhuacheng@hhu.edu.cn)

10 Address: No.1 Xikang Road, Hohai University, Nanjing, China 210098

11

12 **Key Points:**

- 13 • The GRACE CSR mascon product can well represent ACC transport at the Drake
14 • ~~This~~ ACC transport at the Drake Passage has been accelerating during the GRACE era.
15 • The ACC acceleration can be explained by intensified westerly winds and loss of land
16 ice.

17 **Abstract**

18 Previous studies have identified intense climatic change in the Southern Ocean. However, the
19 response of ACC transport to climate change is not fully understood. In this study, by using
20 in-situ ocean bottom pressure (OBP) records and five GRACE products, long-term variations of
21 ACC transport are studied. Our results confirm the reliability of GRACE CSR mascon product in
22 ACC transport estimation at the Drake Passage. Superimposed on interannual variability, ACC
23 transport exhibits an obvious increasing trend ($1.32 \pm 0.07 \text{Sv year}^{-1}$) during the GRACE era.
24 Based on results of a mass-conservation ocean model simulation, we suggest that the
25 acceleration of ACC is associated with intensified westerly winds and loss of land ice in
26 Antarctica.

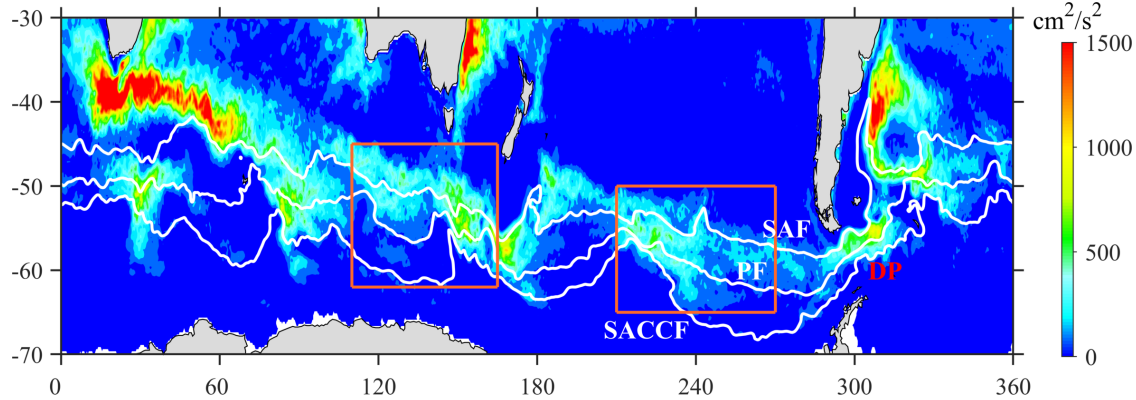
27 **Plain Language Summary**

28 The Southern Ocean is one of the regions most affected by global climatic change. As the
29 dominant circulation in the Southern Ocean, the Antarctic Circumpolar Current (ACC) connects
30 ocean basins, regulating the global climate system and the biogeochemical cycles. However, few
31 studies have explored the response of ACC transport to climate change. In this study, by using
32 OBP data from GRACE satellites, we found that the ACC is accelerating at the Drake passage,
33 due to a combination of intensified westerly winds and loss of land ice in Antarctica.

34 **1. Introduction**

35 The Antarctic Circumpolar Current (ACC), composed of a series of oceanic fronts and a
36 strong eddy field (Figure 1), plays a vital role in regulating the climate system and the carbon
37 cycle (*Meredith et al.*, 2011; *Rintoul*, 2018). Recent studies have identified severe climatic
38 change in the Southern Ocean, manifested in, e.g., subsurface warming (*Roemmich et al.*, 2015),
39 surface freshening (*Haumann et al.*, 2016), and intensified westerly winds (*Thompson et al.*,

40 2011). Thus, it is valuable to explore the response of ACC transport to climatic change in the
 41 Southern Ocean.



42
 43 **Figure 1. Eddy kinetic energy (EKE) calculated using sea surface height anomalies from**
 44 **AVISO data. White contours denote the Subantarctic Front (SAF), Polar Front (PF) and**
 45 **Southern ACC Front (SACCF), respectively. Orange boxes define the areas studied later:**
 46 **110°-170°E, 45°-62°S in the Indian Ocean and 150°-90°W, 50°-65°S in the Pacific. DP**
 47 **denotes the location of the Drake Passage.**

48
 49 Based on geostrophic balance, previous studies have investigated the variations of ACC
 50 transport by using in-situ ocean bottom pressure (OBP) records since 1980s (*Wearn and Baker*,
 51 1980; *Whitworth et al.*, 1982). The Drake Passage, the narrowest constriction of the ACC, has
 52 relatively rich bottom pressure recorders. Based on these OBP records at the Drake Passage,
 53 *Meredith et al.* (2004) estimated the interannual variation of ACC transport. In recent years, there
 54 are many long-term monitoring programs conducted at the passage, such as the cDrake
 55 experiment (*Donohue et al.*, 2016). This experiment contains 46 Current and Pressure-recording
 56 Inverted Echo Sounders (CPIES) sites moored across the Drake Passage from November 2007 to
 57 November 2011 (*Chereskin et al.*, 2012), continuously providing hourly observations of OBP

58 and near-bottom current velocities. Based on these moored instrumentations, *Donohue et*
59 *al.*(2016) examined the mean ACC transport at the Drake Passage. In general, however, these
60 moored instrumentations are still too sparse compared to vastness of the Southern Ocean, and
61 their continuous records are usually no more than a few years.

62 The launch of the Gravity Recovery and Climate Experiment (GRACE) mission provides a
63 unique way to monitor global OBP variabilities (*Tapley et al.*, 2004), which has greatly advanced
64 the understanding of oceanic dynamics, such as the global mean sea level budget (*Chambers et*
65 *al.*, 2017) and regional sea level change (*Cheng and Qi*, 2010). Recently, OBP data based on
66 GRACE satellites are also used to estimate the basin-wide oceanic transports on seasonal to
67 interannual scales (*Liau and Chao*, 2017; *Makowski et al.*, 2015; *Mazloff and Boening*, 2016),
68 and even the deep ocean transport through the Luzon Strait (*Zhu et al.*, 2022). Thus, the OBP
69 data from GARCE satellites have already played an unprecedented role in oceanic transport
70 estimation, and, therefore, long-term sustained monitoring of ocean transports seems achievable.

71 Recent studies also noted some uncertainties in GRACE products, such as discrepancies of
72 OBP estimations among different GRACE products (*Blazquez et al.*, 2018; *Chambers and Bonin*,
73 2012), and the aliasing errors of GRACE products within the periods less than 60 days (*Quinn*
74 *and Ponte*, 2011). Given the active mesoscale activities in the Southern Ocean (*Rintoul and*
75 *Sokolov*, 2001), an assessment of accuracies of different GRACE OBP products is needed before
76 calculating ACC transport.

77 In this paper, variations in the ACC transport are calculated by using both in-situ OBP data
78 and GRACE OBP products. The remainder of this paper is organized as follows. Data and
79 methods are presented in Section 2. In Section 3, we assess the performance of GRACE products,
80 and reveal the accelerating ACC transport under climatic change. In Section 4, we discuss the

81 potential mechanisms of the ACC acceleration.

82

83 **2. Data and methods**

84 In this study, monthly OBP data from five GRACE products are used. Three of them are
85 based on spherical harmonic solutions from Center for Space Research (CSR), Jet Propulsion
86 Laboratory (JPL), and GeoForschungsZentrum Potsdam (GFZ), named as CSR RL06.3, JPL
87 RL06.3 and GFZ RL06.3 products, respectively. The other two products are based on mascon
88 solutions (separating the Earth into equal-area mass concentration cells) from CSR and JPL,
89 named as CSR RL06.2 M and JPL RL06.2 M products, respectively. In this study, the above five
90 GRACE products are referred to as CSR-HR, JPL-HR, GFZ-HR, CSR-MAS and JPL-MAS,
91 respectively. The CSR-HR, JPL-HR and GFZ-HR have the same spatial grids with the horizontal
92 resolution of $1^\circ \times 1^\circ$ (*Chambers and Willis, 2010*). The horizontal resolution of JPL-MAS is
93 $0.5^\circ \times 0.5^\circ$ and the resolution of CSR-MAS is $0.25^\circ \times 0.25^\circ$. The grid point locations of the five
94 GRACE products are shown in Figure S1.

95 In-situ OBP records are obtained from the cDrake experiment. As shown in Figure 2a, 46
96 CPIES sites cover one meridional (black triangles, C line) and three zonal lines [green triangles,
97 Local Dynamics Array (LDA)]. There are also five CPIESs across the Shackleton Fracture Zone
98 (SFZ; magenta triangles, H array), which were placed during the last year. More detailed
99 information of CPIES records is listed in Table S1.

100 The daily absolute dynamic topography (ADT) data are obtained from Archiving Validation
101 and Interpretation of Satellite Data in Oceanography (AVISO) with a $0.25^\circ \times 0.25^\circ$ horizontal
102 resolution. The bathymetry data is obtained from the ETOPO5 global elevation database, which
103 is on a $5' \times 5'$ grid. Surface winds are obtained from ERA5 monthly averaged data obtained from

104 the Asian-Pacific Data Research Center at the University of Hawaii, with a horizontal resolution
105 of $0.25^\circ \times 0.25^\circ$.

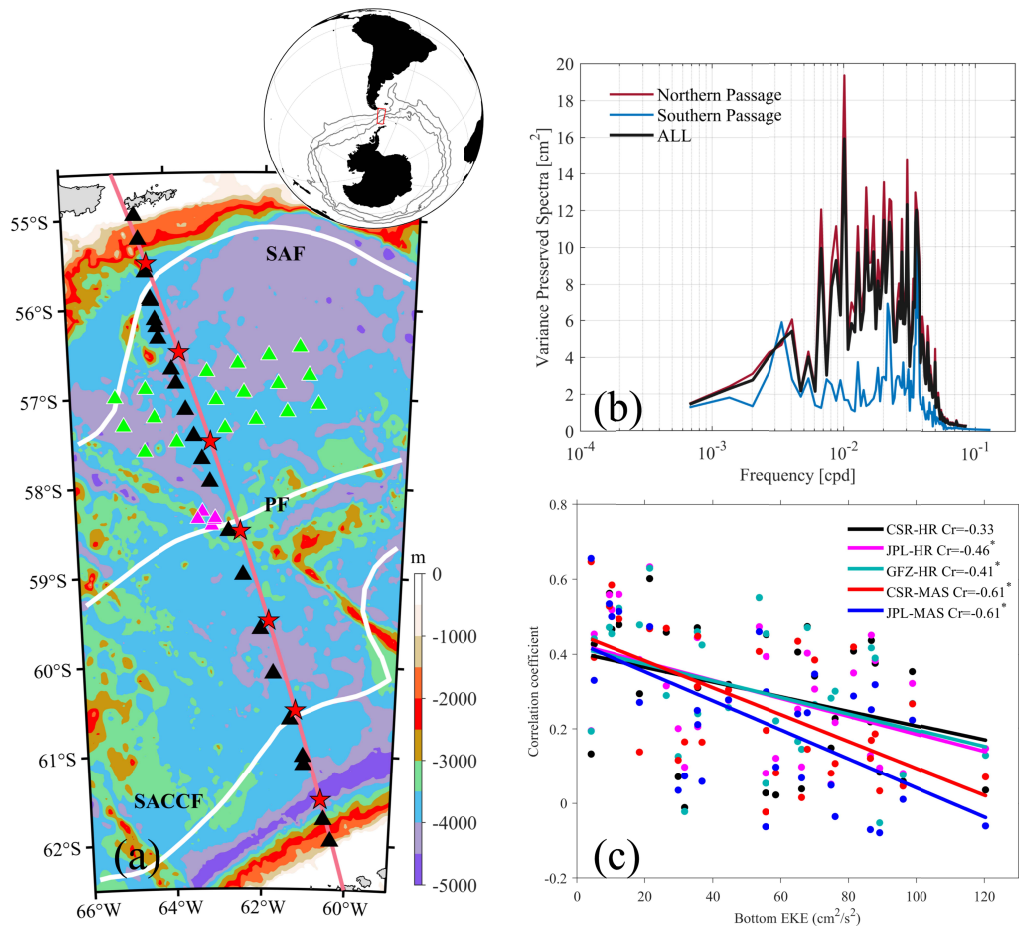
106 When calculating the monthly-mean values of CPIES records, the hourly records are firstly
107 averaged into daily mean, but the daily data are set as missing values if hourly data account for
108 less than half of the day (Figure S1c). Before doing the analysis of monthly mean, a 30-day
109 low-pass Butterworth filter was applied on the daily data to eliminate the higher-frequency
110 signals. The correlation, root-mean-square error (RMSE), and standard deviation (STD) are used
111 to assess the performance of GRACE products in the ACC transport estimation. Student's *t*-test
112 and Mann-Kendall test are used to test the statistical significance of the correlation coefficient
113 and the trend, respectively.

114 The Pressure Coordinate Ocean Model (PCOM) is used in this study. The model is based on
115 mass conservation, rather than the Boussinesq approximation, and can therefore directly simulate
116 the OBP variations (*Huang et al.*, 2001; *Zhang et al.*, 2014). The model is initialized from a
117 resting state with the World Ocean Atlas 2009 (WOA09) and is spun-up with the climatological
118 monthly atmospheric forcing (including sea level pressure, surface wind, surface heat flux and
119 fresh water flux) for 600 years. After the 600-years spin-up integration, the monthly atmospheric
120 forcing is used to force the model from January 1990 to December 2018 (see *Cheng et al.* (2021)
121 for a more detailed model setup). The model output has a $1^\circ \times 1^\circ$ horizontal resolution and 60
122 pressure layers, which has been successfully applied examining OBP variations in the Southern
123 Ocean (*Niu et al.*, 2022; *Qin et al.*, 2022; *Xiong et al.*, 2022).

124 **3. Results**

125 Before evaluating the performance of GRACE products on ACC transport estimation, we
126 firstly explored the OBP mesoscale signals by using in-situ records. Figure 2b shows the power

127 spectrum of daily OBP from CPIES records (30-day low-pass filtered) as a function of frequency.
 128 It is obvious that most of the energy is concentrated in the mesoscale range (30-150 days), which
 129 cannot be well resolved by the monthly averaged GRACE measurements. Considering the
 130 stronger EKE to the north of the PF and weaker EKE to the south, we further calculated the
 131 power spectra of daily OBP in the northern (red line in Figure 2b) and southern passages (blue
 132 line in Figure 2b), respectively. The result reveals a significant north-south difference: there are
 133 intense mesoscale signals in the northern passage but weak in the south, which is consistent with
 134 the spatial distributions of the EKE at the Drake Passage (Figure 1).



135
 136 **Figure 2. (a) Spatial distributions of 46 CPIES at the Drake Passage. The C line and Local**
 137 **Dynamics Array (including A, B, D, E, F and G arrays) are labelled by black and green**
 138 **triangles, respectively, while H arrays are shown with magenta triangles. White lines**

139 **denotes the Subantarctic Front (SAF), Polar Front (PF) and Southern ACC Front**
140 **(SACCF). Red pentagrams are the interpolated site locations studied later. The inset shows**
141 **the location of the study area (red box).** (b) Variance-preserved power spectra as a function
142 **of frequency of OBP (30-day low-pass filtered) at the Drake Passage. Black, red and blue**
143 **lines represent the results in the whole passage, to the north of PF (58.5° S), and to the south**
144 **of PF, respectively.** (c) Scatter plot of bottom EKE and correlation coefficients between
145 **CPIES records and GRACE products at each site. Black, magenta, green, orange, and blue**
146 **dots (regression lines) represent the results using CSR-HR, JPL-HR, GFZ-HR, CSR-MAS,**
147 **JPL-MAS, respectively. * indicates the 95% confidence level of student's *t*-test.**

148
149 To explore whether the performance of GRACE products is affected by local mesoscale
150 signals, we calculated the pointwise correlation between monthly averaged CPIES records and
151 five GRACE products. The OBP time series at each CPIES site from GRACE products are
152 obtained by using linear 2-D interpolation. The interpolation has no impact on the extraction of
153 grid data from different horizontal resolution products in this study (not shown). In general,
154 correlation coefficients are the highest in the southern passage and lowest in the Polar Frontal
155 Zone (Figure S2a-2e). Pointwise RMSEs between monthly averaged CPIES records and five
156 GRACE products were also calculated, and the result is consistent with that of the correlation
157 coefficients (not shown). By using bottom velocity anomalies (30-150-days band-pass filtered)
158 from CPIES, the time-mean bottom EKE was calculated at each site, whose spatial pattern well
159 matches that of the correlation coefficients (Figure S2f). In order to show the relationship in a
160 more straightforward way, the scatter plots of bottom EKE and correlation coefficients between
161 GRACE products and CPIES records are shown in Figure 2c. Regression lines reveal the
162 significant negative relationship between the performance of GRACE products and bottom eddy

163 activities, independent of the different solutions used in GRACE products. The mascon products
 164 show slightly higher regression coefficients than spherical harmonics products, indicating that
 165 the eddy activities have stronger impacts on GRACE products based on mascon solutions. In
 166 general, it could be reasonably deduced that the local mesoscale processes are the key factor for
 167 the spatial inconsistency of the performance of GRACE products at the Drake Passage, and that
 168 mesoscale processes with high EKE are unfavorable for reproducing the monthly OBP
 169 variability in GRACE products. All these need to be considered when calculating ACC transport.

170 Previous studies have proposed two main methods to estimate the zonal transport anomalies
 171 across the selected section based on OBP data (*Makowski et al., 2015; Zhu et al., 2022*):

$$\Delta T_x = -\frac{1}{\bar{f}\rho_0} \int_{-H}^0 (P_N - P_S) dz \quad (1)$$

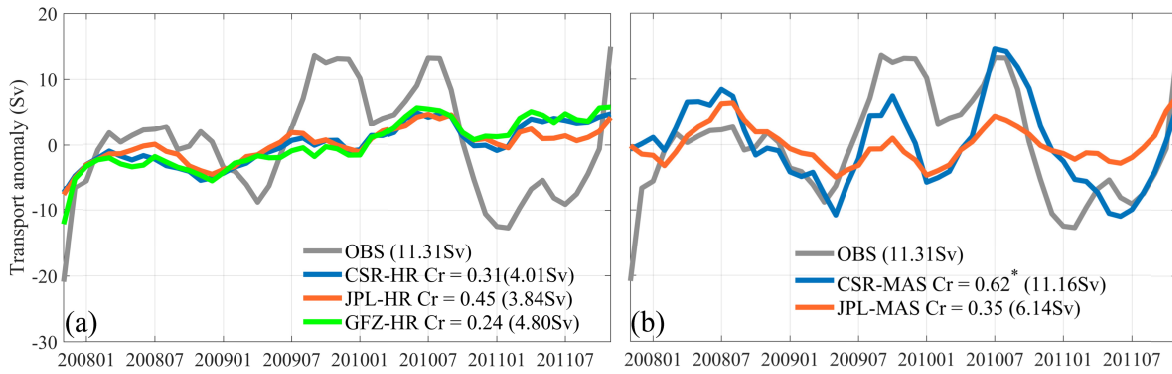
$$\Delta T_x = \int_{y_s}^{y_n} \int_{-H}^0 -\frac{1}{f\rho_0} \frac{\partial P}{\partial y} dz dy \quad (2)$$

172 where f is the Coriolis parameter and ρ_0 is the reference density. H is the topography depth
 173 across the section. P_N and P_S are the OBP time series at the northern and southern boundaries,
 174 respectively. The difference between Equation (1) and (2) is whether to use a constant Coriolis
 175 parameter \bar{f} and whether to integrate the function meridionally. As we mentioned above, the
 176 performance of GRACE products is good in the low EKE regions and unreliable in the high EKE
 177 regions (such as the Polar Frontal Zone). Thus, Equation (1) is chosen in this study, as the
 178 aliasing errors caused by mesoscale activities are considered to be minimal. In order to make the
 179 results independent of the spatial resolution of each GRACE product, the monthly in-situ data
 180 and all five GRACE products were interpolated onto the same cross section with the same grid
 181 points at 1° meridional resolution (red pentagrams in Figure 2a) before calculation.

182 Figure 3 shows the time series of the calculated ACC transport using in-situ observations

183 and five GRACE products. First of all, the results using CSR-HR, JPL-HR, and GFZ-HR
 184 products are an order of magnitude smaller than those using in-situ observations (grey lines),
 185 while the result of CSR-MAS and JPL-MAS products are of the same order of magnitude. In
 186 order to more quantitatively demonstrate the performance of the GRACE product on ACC
 187 transport estimates, we calculated the STD of each time series from GRACE products and the
 188 correlation coefficients between these time series and the in-situ observations. Among all five
 189 GRACE products, the CSR-MAS product has the largest correlation coefficient ($r=0.62$,
 190 significant at the 95% confidence level) with observations, and its STD (11.16Sv) is also the
 191 closest to observations (11.31Sv). All these results indicate that OBP from the CSR-MAS
 192 product is more reliable to monitor the ACC transport variations at the Drake Passage. Therefore,
 193 long-term changes of the ACC transport will be estimated using the CSR-MAS product.

194

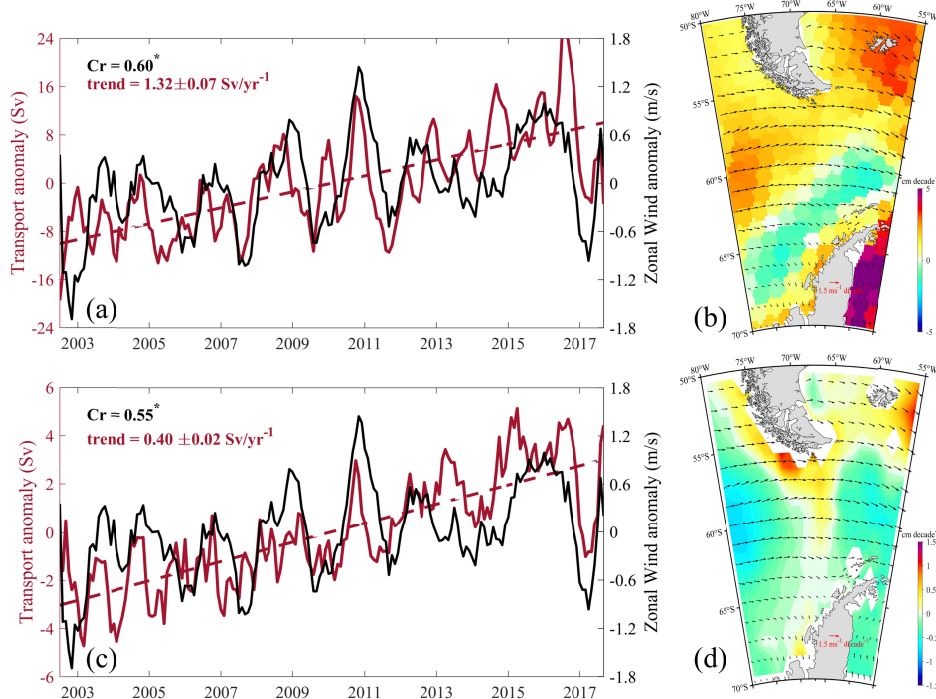


195
 196 **Figure 3. (a) Time series of the ACC transport anomalies smoothed with a five-months**
 197 **moving average filter, calculated using monthly in-situ OBP data (grey line) and**
 198 **GRACE-HR products (color lines). (b) Same as (a) except using GRACE-MAS products**
 199 **(color lines). * indicates the 95% confidence level of student's t -test. Values in () indicate the**
 200 **STD of time series.**

201

202 By using 15-year OBP data from the CSR-MAS product, the ACC transport variations at

203 the Drake Passage from April 2002 to July 2017 are calculated (the red line in Figure 4a).
 204 Despite the interannual variability, there is a clear increasing trend in ACC flow (the pink line,
 205 $1.32 \pm 0.07 \text{ Sv year}^{-1}$, significant at the 95% confidence level). Considering the controlling effect
 206 of the westerly wind in the Southern Ocean, the variation in zonal-mean surface wind velocity
 207 (averaged between 50°S - 65°S) was calculated using ERA5 monthly averaged data (the black line
 208 in Figure 4a). The correlation coefficient between zonal-mean wind velocity and the calculated
 209 ACC transport is 0.60, significant at the 95% confidence level. The correlation drops to 0.52
 210 when linear trends are removed from both time series (Figure S3). Figure 4b shows the spatial
 211 distribution of linear trend of surface winds (arrows) and OBP anomalies (color) at the Drake
 212 Passage. It is obvious that the westerly wind has strengthened over the Southern Ocean, and the
 213 trend of OBP shows a “dipole structure” at the Drake Passage, increasing in the north and
 214 decreasing in the south, which promotes the enhancement of the ACC.



215
 216 **Figure 4. (a)** Time series of the ACC transport anomalies using CSR-MAS OBP product
 217 (red line) and zonal-mean surface wind (black line) from ERA5 data, smoothed with a

218 **five-months moving average filter. (b) Linear trend of ERA5 surface wind (arrows) and**
219 **OBP (shading). (c) and (d) are same as (a) and (b) but using PCOM output. * indicates the**
220 **95% confidence level of student's *t*-test.**

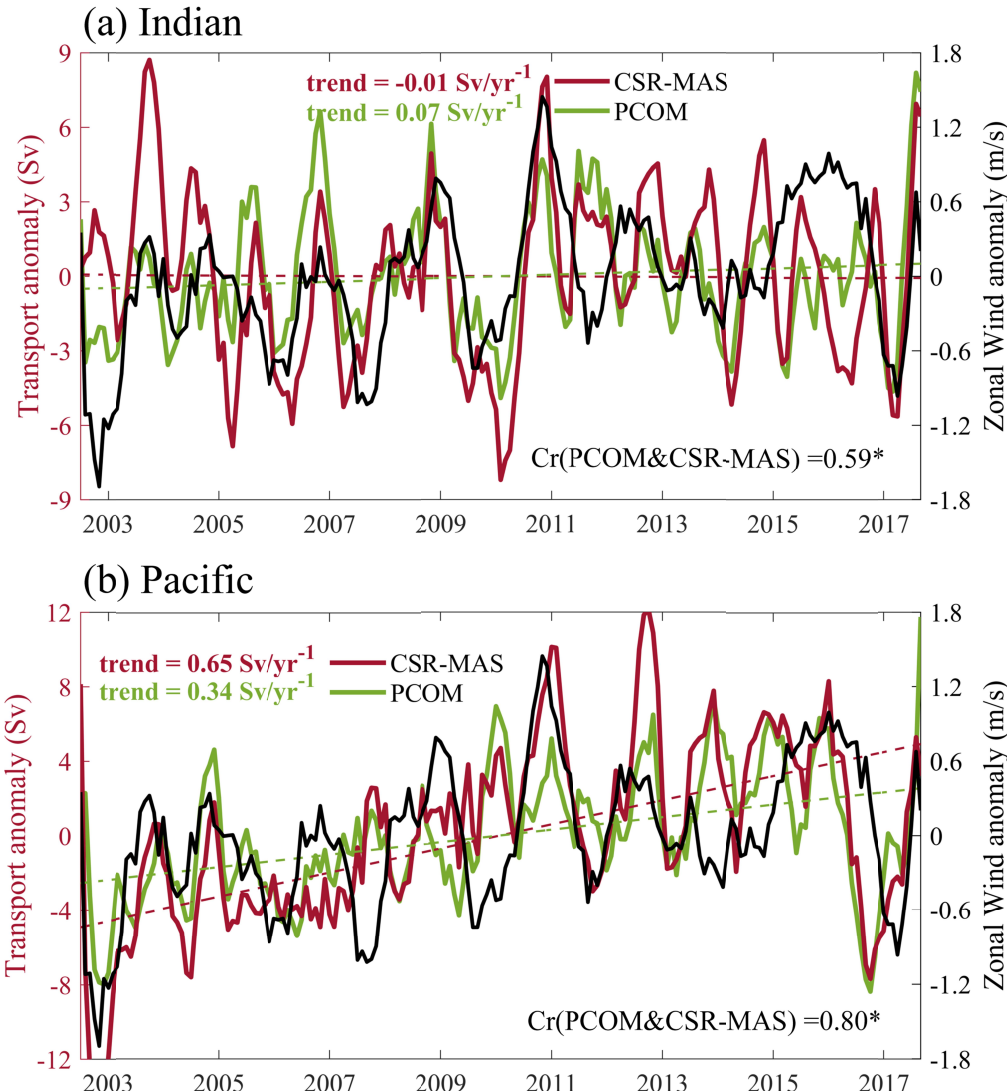
221

222 Although the calculated ACC transport shows a good correlation with the zonal-mean wind,
223 there is no direct evidence that the accelerating ACC is mainly caused by the strengthening of
224 westerly winds. Previous studies suggested that the westerly wind dominates the ACC transport
225 variations on timescale from days to years (*Hughes et al.*, 1999; *Meredith et al.*, 2004). On
226 timescales longer than a few years, intrinsic variability in the Southern Ocean readjusts the ACC
227 (*Hogg and Blundell*, 2006). To examine the relationship between ACC trend and the intensifying
228 westerly winds, in this study the PCOM was employed, forced only by surface wind stress from
229 monthly ERA5 data, without changes of heat or freshwater flux. Using the same method as for
230 the GRACE products, we calculated the time series of ACC transport simulated by PCOM. As
231 shown in Figure 4c, a good correlation between ACC transport and zonal wind is found. In
232 addition, the enhancement of the westerly winds leads to increased OBP in the northern passage
233 and decreased OBP in the southern passage along the Antarctic Peninsula (Figure 4d). Such
234 north-south gradient of the OBP in turn accelerates the ACC at the Drake Passage. The ACC
235 transport derived from the PCOM simulation is significantly correlated with that derived from
236 CSR-MAS product ($r=0.72$, significant at the 95% confidence level, Figure S3), while the
237 amplitude and the rise rate are about one third of those from CSR-MAS product.

238 *Hsu and Velicogna* (2017) suggested that glacier loss of the Antarctica could regulate the
239 mass redistribution in the Southern Ocean, leading to significant OBP gradients near the Drake
240 Passage and weak gradients in the other regions (Figure 1 in their paper). Thus, we also

241 compared the zonal-averaged ACC transport variations in the Indian (110° - 170° E, 45° - 62° S) and
242 Pacific (150° - 90° W, 50° - 65° S) oceans, with their northern and southern boundaries away from
243 the high EKE regions (orange boxes in Figure 1). As shown in Figure 5, the PCOM result
244 exhibits a good agreement with that from CSR-MAS product, with high correlation coefficients
245 ($r=0.59$ in the Indian Ocean and $r=0.80$ in the Pacific, significant at the 95% confidence level),
246 same order of amplitude, and similar trend change of ACC transport. In summary, it could be
247 concluded that the PCOM can well characterize the response of ACC transport to the westerly
248 wind change at the Drake Passage, and the difference in ACC trends between GRACE product
249 and PCOM output may be related to the glacier loss of the Antarctica.

250



251
252 **Figure 5. Time series of the ACC transport anomalies calculated using OBP data in the (a)**
253 **Indian and (b) Pacific oceans, smoothed with a five-months moving average filter. Red and**
254 **green lines represent the result from CSR-MAS product and PCOM output, respectively.**
255 **Dash lines represent the linear trend of ACC transport. Black lines in (a) and (b) represent**
256 **the zonal-mean surface wind variations from ERA5 data, smoothed with a five-months**
257 **moving average filter. * indicates the 95% confidence level of student's *t*-test.**
258

259 **4. Conclusions and discussions**

260 This study investigates variations of ACC transport at the Drake Passage using in-situ OBP
261 records, five GRACE products, and the PCOM simulation. Our results reveal that the GRACE
262 CSR mascon product closely resembles the in-situ OBP data, and is therefore favorable to
263 estimate ACC transport at the Drake Passage. Based on 15-year CSR mascon product, the
264 changes of ACC transport in the context of climatic change is studied. ACC transport at the
265 Drake Passage shows an obvious increasing trend of $1.32 \pm 0.07 \text{Sv yr}^{-1}$. Sensitivity experiment
266 using PCOM indicates that the intensified westerly winds can partially explain the ACC
267 acceleration at the Drake Passage. The glacial loss of Antarctica may account for the residual
268 parts of the acceleration.

269 Although the PCOM model can partially capture the increasing trend of ACC transport,
270 there are some differences of OBP trends between PCOM results and GRACE measurements. As
271 shown in Figure 4b, except for the southern passage, OBP trends from CSR-MAS product are
272 mostly positive at the Drake Passage, with a maximum value at $75^{\circ}\text{W}, 60^{\circ}\text{S}$. In contrast, OBP
273 trends from PCOM are mostly negative in the southern passage, with a minimum value at $75^{\circ}\text{W},$
274 60°S (Figure 4d). This difference in spatial distribution may be due to the absence of glacier loss
275 in the Antarctica. Thus, the meridional OBP gradient in the model is presumably due to mass
276 redistribution caused by wind-induced Ekman transport. This result confirms previous findings
277 (*Hsu and Velicogna, 2017*) stating that mass redistribution due to glaciers loss accounts for most
278 OBP trend at the Drake Passage during the GRACE era. This can explain the faster increasing
279 trend of the ACC transport estimated from CSR-MAS OBP product.

280 At present, the response of the ACC to climatic change (changes in westerly wind and
281 buoyancy forcing) has received increasing attention (*Rintoul, 2018*). There is no doubt that in the
282 context of intensified westerly winds, kinetic energies have increased in the Southern Ocean (*Hu*

283 *et al.*, 2020). However, it is still unclear how and where these additional energies are stored.
284 Model-based studies reveal that the ACC transport is insensitive to the increase of the westerly
285 wind (*Downes et al.*, 2011), and the additional energy is transferred into mesoscale eddies
286 (*Marshall et al.*, 2017), which is known as the “eddy saturation” hypothesis (*Munday et al.*,
287 2013). However, based on altimetry crossover measurements and ocean reanalysis product,
288 *Zhang et al.* (2021) found that EKE does not increase coherently across the Southern Ocean.
289 This contradiction may be due to the fact that changes of kinetic energies in the deep ocean are
290 not considered in these studies. Based on OBP data, our results indicate that ACC is accelerating
291 in the deep ocean, at least at the Drake Passage. Therefore, more observational research in the
292 deep Southern Ocean are needed to improve our understanding of energy transport pathways in
293 the Southern Ocean, especially in the context of global warming.

294 **Acknowledgments**

295 This research was supported by the Natural Science Foundation of China (Grant no.41876002)
296 and Postgraduate Research & Practice Innovation Program of Jiangsu Province (grant
297 KYCX22_0585).

298 **Data Availability Statement**

299 The GRACE data are available at <https://podaac.jpl.nasa.gov/GRACE> and
300 https://www2.csr.utexas.edu/grace/RL06_mascons.html. In-situ bottom pressure records of
301 cDrake experiment are obtained from the University of Rhode Island Web site
302 (<http://www.po.gso.uri.edu/dynamics/Drake/index.html>). Absolute dynamic topography data are
303 available from the Copernicus Marine Environment Monitoring Service Web site
304 (https://resources.marine.copernicus.eu/product-detail/SEALEVEL_GLO_PHY_L4_MY_008_047/DATA-ACCESS). The ETOPO5 database is obtained from the National Centers for

306 Environmental Information Web site (<https://www.ngdc.noaa.gov/mgg/global/etopo5.HTML>).
307 ERA5 monthly averaged wind data are available from Asian Pacific data research center at the
308 University of Hawaii Web site (<http://apdrc.soest.hawaii.edu/las/v6/constrain?var=16447>).
309

310 References

- 311 Blazquez, A., B. Meyssignac, J. M. Lemoine, E. Berthier, A. Ribes, and A. Cazenave (2018),
312 Exploring the uncertainty in GRACE estimates of the mass redistributions at the Earth
313 surface: implications for the global water and sea level budgets, *Geophysical Journal
314 International*, 215(1), 415-430, doi: 10.1093/gji/ggy293.
- 315 Chambers, D. P., and J. K. Willis (2010), A Global Evaluation of Ocean Bottom Pressure from
316 GRACE, OMCT, and Steric-Corrected Altimetry, *Journal Of Atmospheric And Oceanic
317 Technology*, 27(8), 1395-1402, doi: 10.1175/2010jtecho738.1.
- 318 Chambers, D. P., and J. A. Bonin (2012), Evaluation of Release-05 GRACE time-variable gravity
319 coefficients over the ocean, *Ocean Science*, 8(5), 859-868, doi: 10.5194/os-8-859-2012.
- 320 Chambers, D. P., A. Cazenave, N. Champollion, H. Dieng, W. Llovel, R. Forsberg, K. von
321 Schuckmann, and Y. Wada (2017), Evaluation of the Global Mean Sea Level Budget
322 between 1993 and 2014, *Surveys In Geophysics*, 38(1), 309-327, doi:
323 10.1007/s10712-016-9381-3.
- 324 Cheng, X., N. Ou, J. Chen, and R. X. Huang (2021), On the seasonal variations of ocean bottom
325 pressure in the world oceans, *Geoscience Letters*, 8(1), doi: 10.1186/s40562-021-00199-3.
- 326 Cheng, X. H., and Y. Q. Qi (2010), On steric and mass-induced contributions to the annual
327 sea-level variations in the South China Sea, *Global And Planetary Change*, 72(3), 227-233,
328 doi: 10.1016/j.gloplacha.2010.05.002.

- 329 Chereskin, T. K., K. A. Donohue, and R. Watts (2012), cDrake: Dynamics and Transport of the
330 Antarctic Circumpolar Current in Drake Passage, *Oceanography*, 25(3), 134-135, doi:
331 10.5670/oceanog.2012.86.
- 332 Donohue, K. A., K. L. Tracey, D. R. Watts, M. P. Chidichimo, and T. K. Chereskin (2016), Mean
333 Antarctic Circumpolar Current transport measured in Drake Passage, *Geophysical Research
Letters*, 43(22), doi: 10.1002/2016gl070319.
- 335 Downes, S. M., A. S. Budnick, J. L. Sarmiento, and R. Farneti (2011), Impacts of wind stress on
336 the Antarctic Circumpolar Current fronts and associated subduction, *Geophysical Research
Letters*, 38(11), n/a-n/a, doi: 10.1029/2011gl047668.
- 338 Haumann, F. A., N. Gruber, M. Münnich, I. Frenger, and S. Kern (2016), Sea-ice transport
339 driving Southern Ocean salinity and its recent trends, *Nature*, 537(7618), 89-92, doi:
340 10.1038/nature19101.
- 341 Hogg, A. M. C., and J. R. Blundell (2006), Interdecadal Variability of the Southern Ocean,
342 *Journal of Physical Oceanography*, 36(8), 1626-1645, doi: 10.1175/JPO2934.1.
- 343 Hsu, C.-W., and I. Velicogna (2017), Detection of sea level fingerprints derived from GRACE
344 gravity data, *Geophysical Research Letters*, 44(17), 8953-8961, doi:
345 10.1002/2017gl074070.
- 346 Hu, S., J. Sprintall, C. Guan, M. J. McPhaden, F. Wang, D. Hu, and W. Cai (2020),
347 Deep-reaching acceleration of global mean ocean circulation over the past two decades,
348 *Science advances*, 6(6), eaax7727, doi: 10.1126/sciadv.aax7727.
- 349 Huang, R., X. Jin, and X. Zhang (2001), An oceanic general circulation model in pressure
350 coordinates, *Advances in Atmospheric Sciences*, 18(1), 1-22, doi:
351 10.1007/s00376-001-0001-9.

- 352 Hughes, C. W., M. P. Meredith, and K. J. Heywood (1999), Wind-Driven Transport Fluctuations
353 through Drake Passage: A Southern Mode, *Journal of Physical Oceanography*, 29(8),
354 1971-1992, doi: 10.1175/1520-0485(1999)029<1971:WDTFTD>2.0.CO;2.
- 355 Liau, J. R., and B. F. Chao (2017), Variation of Antarctic circumpolar current and its
356 intensification in relation to the southern annular mode detected in the time-variable gravity
357 signals by GRACE satellite, *Earth Planets And Space*, 69, 1-9, doi:
358 10.1186/s40623-017-0678-3.
- 359 Makowski, J. K., D. P. Chambers, and J. A. Bonin (2015), Using ocean bottom pressure from the
360 gravity recovery and climate experiment (GRACE) to estimate transport variability in the
361 southern Indian Ocean, *Journal Of Geophysical Research-Oceans*, 120(6), 4245-4259, doi:
362 10.1002/2014jc010575.
- 363 Marshall, D. P., M. H. P. Ambaum, J. R. Maddison, D. R. Munday, and L. Novak (2017), Eddy
364 saturation and frictional control of the Antarctic Circumpolar Current, *Geophysical
365 Research Letters*, 44(1), 286-292, doi: <https://doi.org/10.1002/2016GL071702>.
- 366 Mazloff, M. R., and C. Boening (2016), Rapid variability of Antarctic Bottom Water transport
367 into the Pacific Ocean inferred from GRACE, *Geophysical Research Letters*, 43(8),
368 3822-3829, doi: 10.1002/2016gl068474.
- 369 Meredith, M. P., P. L. Woodworth, C. W. Hughes, and V. Stepanov (2004), Changes in the ocean
370 transport through Drake Passage during the 1980s and 1990s, forced by changes in the
371 Southern Annular Mode, *Geophysical Research Letters*, 31(21), doi:
372 <https://doi.org/10.1029/2004GL021169>.
- 373 Meredith, M. P., et al. (2011), Sustained Monitoring Of the Southern Ocean at Drake Passage:
374 Past Achievements And Future Priorities, *Reviews of Geophysics*, 49(4), doi:

- 375 10.1029/2010rg000348.
- 376 Munday, D. R., H. L. Johnson, and D. P. Marshall (2013), Eddy Saturation of Equilibrated
377 Circumpolar Currents, *Journal of Physical Oceanography*, 43(3), 507-532, doi:
378 10.1175/JPO-D-12-095.1.
- 379 Niu, Y., X. Cheng, J. Qin, N. Ou, C. Yang, and D. Huang (2022), Mechanisms of Interannual
380 Variability of Ocean Bottom Pressure in the Southern Indian Ocean, *Frontiers in Marine
381 Science*, 9.
- 382 Qin, J., X. Cheng, C. Yang, N. Ou, and X. Xiong (2022), Mechanism of interannual variability of
383 ocean bottom pressure in the South Pacific, *Climate Dynamics*, doi:
384 10.1007/s00382-022-06198-0.
- 385 Quinn, K. J., and R. M. Ponte (2011), Estimating high frequency ocean bottom pressure
386 variability, *Geophysical Research Letters*, 38(8), n/a-n/a, doi: 10.1029/2010gl046537.
- 387 Rintoul, S. R. (2018), The global influence of localized dynamics in the Southern Ocean, *Nature*,
388 558(7709), 209-218, doi: 10.1038/s41586-018-0182-3.
- 389 Rintoul, S. R., and S. Sokolov (2001), Baroclinic transport variability of the Antarctic
390 Circumpolar Current south of Australia (WOCE repeat section SR3), *Journal Of
391 Geophysical Research-Oceans*, 106(C2), 2815-2832, doi: 10.1029/2000jc900107.
- 392 Roemmich, D., J. Church, J. Gilson, D. Monselesan, P. Sutton, and S. Wijffels (2015), Unabated
393 planetary warming and its ocean structure since 2006, *Nature Climate Change*, 5(3),
394 240-245, doi: 10.1038/nclimate2513.
- 395 Tapley, B. D., S. Bettadpur, J. C. Ries, P. F. Thompson, and M. M. Watkins (2004), GRACE
396 measurements of mass variability in the Earth system, *Science*, 305(5683), 503-505, doi:
397 10.1126/science.1099192.

- 398 Thompson, D. W. J., S. Solomon, P. J. Kushner, M. H. England, K. M. Grise, and D. J. Karoly
399 (2011), Signatures of the Antarctic ozone hole in Southern Hemisphere surface climate
400 change, *Nature Geoscience*, 4(11), 741-749, doi: 10.1038/ngeo1296.
- 401 Wearn, R. B., and D. J. Baker (1980), Bottom pressure measurements across the Antarctic
402 circumpolar current and their relation to the wind, *Deep Sea Research Part A.*
403 *Oceanographic Research Papers*, 27(11), 875-888, doi:
404 [https://doi.org/10.1016/0198-0149\(80\)90001-1](https://doi.org/10.1016/0198-0149(80)90001-1).
- 405 Whitworth, T., W. D. Nowlin, and S. J. Worley (1982), The Net Transport of the Antarctic
406 Circumpolar Current through Drake Passage, *Journal of Physical Oceanography*, 12(9),
407 960-971, doi: 10.1175/1520-0485(1982)012<0960:TNTOTA>2.0.CO;2.
- 408 Xiong, X., X. Cheng, N. Ou, T. Feng, J. Qin, X. Chen, and R. X. Huang (2022), Dynamics of
409 seasonal and interannual variability of the ocean bottom pressure in the Southern Ocean,
410 *Acta Oceanologica Sinica*, 41(5), 78-89, doi: 10.1007/s13131-021-1878-z.
- 411 Zhang, Y., Y. Lin, and R. Huang (2014), A climatic dataset of ocean vertical turbulent mixing
412 coefficient based on real energy sources, *Science China Earth Sciences*, 57(10), 2435-2446,
413 doi: 10.1007/s11430-014-4904-6.
- 414 Zhang, Y., D. Chambers, and X. Liang (2021), Regional Trends in Southern Ocean Eddy Kinetic
415 Energy, *Journal of Geophysical Research: Oceans*, 126(6), doi: 10.1029/2020jc016973.
- 416 Zhu, Y., J. Yao, T. Xu, S. Li, Y. Wang, and Z. Wei (2022), Weakening Trend of Luzon Strait
417 Overflow Transport in the Past Two Decades, *Geophysical Research Letters*, 49, doi:
418 10.1029/2021GL097395.
- 419